



Remote Sensing Based Rapid Assessment of Flood Crop Damage Using Novel Disaster Vegetation Damage Index (DVDI)

Md. Shahinoor Rahman¹ · Liping Di¹ · Eugene Yu¹ · Li Lin¹ · Zhiqi Yu¹

Accepted: 14 September 2020 / Published online: 2 November 2020
© The Author(s) 2020

Abstract Accurate crop-specific damage assessment immediately after flood events is crucial for grain pricing, food policy, and agricultural trade. The main goal of this research is to estimate the crop-specific damage that occurs immediately after flood events by using a newly developed Disaster Vegetation Damage Index (DVDI). By incorporating the DVDI along with information on crop types and flood inundation extents, this research assessed crop damage for three case-study events: Iowa Severe Storms and Flooding (DR 4386), Nebraska Severe Storms and Flooding (DR 4387), and Texas Severe Storms and Flooding (DR 4272). Crop damage is assessed on a qualitative scale and reported at the county level for the selected flood cases in Iowa, Nebraska, and Texas. More than half of flooded corn has experienced no damage, whereas 60% of affected soybean has a higher degree of loss in most of the selected counties in Iowa. Similarly, a total of 350 ha of soybean has moderate to severe damage whereas corn has a negligible impact in Cuming, which is the most affected county in Nebraska. A total of 454 ha of corn are severely damaged in Anderson County, Texas. More than 200 ha of alfalfa have moderate to severe damage in Navarro County, Texas. The results of damage assessment are validated through the NDVI profile and yield loss in percentage. A linear relation is found between DVDI values and crop yield loss. An R^2 value of 0.54 indicates the potentiality of DVDI for rapid crop damage estimation. The results also indicate the association between DVDI class and crop yield loss.

Keywords Crop damage · Disaster vegetation damage index (DVDI) · Flood inundation · Rapid assessment · Remote sensing

1 Introduction

Flood causes significant crop damage around the globe every year (FAO 2015). The frequency and intensity of floods have increased because of recent climate change (Aerts and Botzen 2011; Bouwer 2011; Field et al. 2012; Hirabayashi et al. 2013). The Food and Agriculture Organization of the United Nations estimates that more than 93 thousand hectares of cropland and 1.6 million tons of crops are damaged by flooding in a decade (2003–2013), which accounts for more than half of aggregated crops damaged by natural hazards and disasters (FAO 2015). Crops are highly vulnerable to flooding for two reasons: crop fields are usually located in fertile flood plains; and the agricultural sector is weakly protected by flood protection measures (Brémond and Agenais 2013). Flood damage and loss assessment have become more important because of recent paradigm shifts in flood management from traditional physical-based management approach to risk management (Merz et al. 2010; Gerl et al. 2016; Adnan et al. 2020). Flood crop loss assessment is not only crucial for understanding the direct loss of crop yield, but also essential for the aftermath of trade flows of agricultural commodities, sectoral growth, and ultimately national economy (Del Ninno et al. 2003; FAO 2015). Accurate crop loss assessment after flood events is essential for crop pricing, damage compensation, financial appraisal for the insurance sector, yield assessment, food trade impact assessment, mitigation measures, and comprehensive risk analysis.

✉ Liping Di
ldi@gmu.edu

¹ Center for Spatial Information Science and Systems, George Mason University, Fairfax, VA 22030, USA

Therefore, the information on flooded acreage and the degree of damage are the most essential aspects of all flood-related decision support systems.

The flood assessment model developed by the World Meteorological Organization and the Global Water Partnership includes a three-stage assessment: rapid assessment, early recovery assessment, and in-depth assessment (Di et al. 2017). Since the detailed evaluation is time-consuming, early recovery assessment and comprehensive assessment may not be able to support immediate policy and decision processes. Rapid assessment of flood-affected cropland acreage, however, can be helpful for early action to reduce the disaster risk. One very general approach for rapid flood crop loss assessment is to estimate the flooded acreage of cropland (Cressman et al. 1988). A more specific approach than a general approach is crop-specific flooded acreage estimation (Citeau 2003; Dutta et al. 2003; Zhu et al. 2007; Förster et al. 2008). Another approach is the loss assessment using crop condition and growth stage information. In the latter approach among the three common approaches, relative damage can be assessed quickly by analyzing crop conditions by means of the vegetation indices (VIs) of crops (Ahmed et al. Ahmed 2017; Shrestha et al. 2017).

Figure 1 illustrates the conceptual framework for the estimation of flood crop loss using remote sensing-derived crop type, crop condition profile, and flood inundation extent. The traditional field survey-based system is a cost ineffective, labor intensive, noncontinuous, time consuming, and incomplete technique for gathering required information over vast agricultural areas (Tapia-Silva et al. 2011; Ahmed et al. 2017; Di et al. 2017). Besides, field survey is very challenging at almost any time of the year (Merz et al. 2010; Brémond and Agenais 2013). Spaceborne remote sensing brings cost-effective and efficient solutions to the rapid gathering of information on flood

extent, crop types, and crop condition profiles (Opolot 2013; Schumann and Moller 2015; Lin et al. 2016; Rahman and Di 2017). Satellite remote sensing data have been successfully used for the monitoring of crop condition profile (Yu et al. 2013; Di et al. 2017). Moreover, remote sensing is the only feasible option for in-season mapping of crop types over agricultural land (Mosleh et al. 2015; Rahman et al. 2019).

The degree of crop damage can be assessed either by comparing vegetation indices before and after a flood event or by comparing current crop conditions with the historical condition. Many vegetation indices have been developed for crop condition monitoring, including NDVI (Normalized Difference Vegetation Index), EVI (Enhanced Vegetation Index), RVI (Ratio Vegetation Index), SAVI (Soil Adjusted Vegetation Index), OSAVI (Optimized Soil Adjusted Vegetation Index), VCI (Vegetation Condition Index), MCVI (Mean Vegetation Condition Index), RMVCI (Ratio to Median Vegetation Condition Index), and LAI (Leaf Area Index). Although most of these vegetation indices were originally developed for the monitoring of crop response to drought, many recent studies have used them for flood damage assessment. These VIs can be broadly categorized into two groups: VIs directly derived from remote sensing bands, for example, NDVI; and VIs not directly derived from remote sensing bands, for example, VCI, which compares the current NDVI to historic NDVI (Rahman and Di 2020). The NDVI, which is one of the most common VIs, is the ratio between the infrared and visible red bands of the electromagnetic spectrum. A NDVI measures the greenness of vegetation, which is directly correlated with vegetation health. Because NDVI is also the primary input for the calculation of other Vis, Kogan et al. (2012) proposed the VCI by further normalization of NDVI with historic maximum and minimum NDVIs. The idea behind VCI is to capture

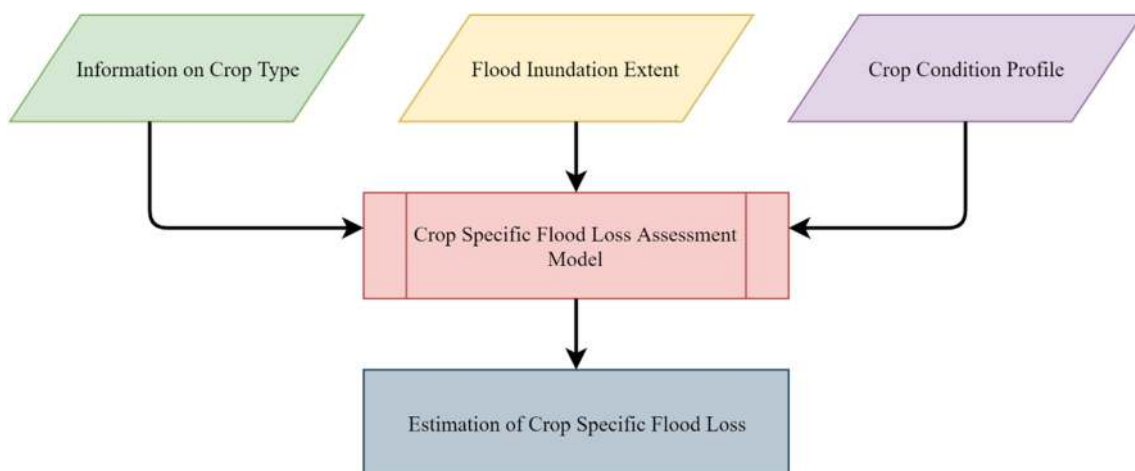


Fig. 1 Framework for crop-specific flood loss assessment using remote sensing technology

relative NDVI change with respect to historical NDVI at a given location. Another VCI, MVCI, considers the mean NDVI instead of maximum and minimum NDVI from historic NDVI time-series data. Although both mean and median express the central tendency of data, the mean is sensitive to outliers. Daily NDVI is often contaminated by clouds, which results in unreliable mean NDVI. Therefore to avoid the effect of cloud and other noise on NDVI, a modified VCI (mVCI) that uses median NDVI instead of mean NDVI can be used for monitoring vegetation conditions (Di, Yu et al. 2018). Yu et al. (2013) examined various vegetation indices (VIs) for remote sensing-based flood damage estimation and concluded that all vegetation indices can detect flood impact on crops; but their performances are varied from case to case. Shrestha et al. (2013) compared the MODIS (Moderate Resolution Imaging Spectroradiometer) NDVI time series with historical median NDVI between 2000 and 2014 to show the impact of floods on crops. Liu et al. (2018) developed a regression model using multivariate VIs (for example, NDVI, EVI, RVI, OSAVI, MTVI2,¹ EVI2,² and GNDVI³), leaf area index (LAI), and above-ground biomass to assess the damage on winter wheat. Chejarla et al. (2016) assessed crop loss by comparing crop biomass before and after flood events.

Therefore, flood crop damage can be rapidly assessed by the change in the crop conditions profile before and after a flood event. Di, Yu et al. (2018) proposed a novel index called Disaster Vegetation Damage Index (DVDI) to measure crop/vegetation damage by disaster events. This proposed novel technique relies on mVCI (median Vegetation Condition Index) before and after disaster events. Therefore, this method can be useful for remote sensing-based rapid assessment of flood crop damage. Recent studies have shown that DVDI is an effective index for rapidly measuring vegetation damage due to natural hazard-induced disasters (Di, Guo et al. 2018; Lu et al. 2020). This study aims to use the newly developed DVDI to examine the crop-specific degree of flood crop damage for selected case studies by incorporating three primary information: crop types, crop condition, and flood extents.

2 Materials and Methods

This research follows a step by step workflow to derive three required sets of information for crop-specific damage assessment, including crop types, flood extents, and crop condition profiles from Earth observation. Section 2.1 provides a brief introduction of three selected case studies.

¹ Modified Triangular Vegetation Index2.

² Enhanced Vegetation Index2.

³ Green Normalized Difference Vegetation Index.

Sections 2.2–2.4 illustrate the methodological procedure for the mapping of crop types, flood extent mapping, and rapid crop damage assessment using DVDI. Section 2.5 presents the validation of the damage assessment.

2.1 Study Areas

Three recent flood cases are chosen for this study from among the Federal Emergency Management Agency (FEMA)'s major disaster declarations. These cases are: Iowa Severe Storms and Flooding (Major Disaster Declaration Number DR 4386; FEMA 2018a); Nebraska Severe Storms and Flooding (Major Disaster Declaration Number DR 4387; FEMA 2018b); and Texas Severe Storms and Flooding (Major Disaster Declaration Number DR 4272; FEMA 2016). The case studies are selected from recent (within three years before 2019) flood events. These cases are chosen because of their incident period in the middle of the crop growing season and the severity of potential crop damage. These events impacted a vast amount of arable land, which is another important aspect of the selection of these cases. Counties are selected for crop-specific quantitative damage assessment based on their exposure (flood extent) to the corresponding flood case.

Iowa and Nebraska are Midwestern states in the United States, and are located on the east and west banks of the Missouri River, respectively. Geographically, these two states are part of the Great Plains, and about 90% of their land is devoted to agriculture because of the high fertility of the soils in this region. These states are also considered as the Corn Belt region of the United States due to their high proportion of corn cultivation. The third case study area, Texas, is located in the central-south part of the United States. According to the United States Department of Agriculture (USDA), Iowa, Nebraska, and Texas are the top three grain-producing states after California, and produce 8.10%, 6.20%, and 5.8% respectively of agricultural commodities in the United States (USDA-ERS 2016).

DR 4386 is a FEMA declared disaster event in Iowa, which occurred between 6 June and 2 July 2018. This event impacted 31 counties in the northwestern part of the state. Six counties, Osceola, Kossuth, Clay, Palo Alto, Humboldt, and Wright, are selected for detailed assessment. These six counties are selected based on the total area of flood extents. DR 4387 is a FEMA declared disaster event in Nebraska, which occurred between 17 June and 1 July 2018. This event impacted 11 counties with varying severity, mostly located in the northeastern part of the state. The six most affected counties by this flood event are Dixon, Dakota, Wayne, Thurston, Cuming, and Colfax. DR 4272 is a FEMA declared disaster event in Texas, which occurred between 22 May and 24 June 2016, and impacted more than 20 counties in the southeastern part of Texas.

Ellis, Navarro, Anderson, and Robertson are the most affected counties based on the total area of flood extents. These four counties are selected in this case study for detailed assessment for the 2016 flood event.

2.2 Rapid Mapping of Crop Types

Field level crop type information is crucial for the rapid assessment of crop-specific damage. However, census-based, crop-type information is not readily available during the crop growing season. For instance, the USDA crop data layer (CDL) provides crop-specific land cover products for the United States, which is available at the end of the growing season. In-season, crop-specific damage assessment cannot utilize CDL because of the data's delayed release. Therefore, two major approaches can be considered for the rapid gathering of in-season crop type information: remote sensing-based, in-season mapping of crop types; and machine learning-based prediction of crop types at field level. The detailed methodological approaches of remote sensing-based crop mapping can be found in a previous study by Rahman et al. (2019). One major drawback of optical remote sensing is the inability to see through clouds, which may hinder in-season crop mapping. Since farmers may rotate their crops, the pattern of crop rotation may be useful for crop mapping without analyzing remote sensing imageries. Thus, the second approach is the use of machine learning for the prediction of field-level crop types using crop rotation. Our study used Markov chain modeling to predict field level crop types in order to support crop-specific flood damage assessment.

Since CDL provides historical crop types at pixel level over more than 10 years, crop rotation pattern at parcel level can be used for prediction modeling. Information on crop types planted in a field over many years can be seen as a discrete sequence. The prediction of the next item in the given sequence can be the approach employed to predict crop types for the next year. Markovian logic is frequently used for prediction models that rely on learning from sequential states of variables. Aurbacher and Dabbert (2011) generate crop sequences in land-use models using maximum entropy and Markov chains. They found that the Markov chain approach is more suitable than normal simple stochastic modeling for cropping sequence prediction in their case study on German croplands. Similarly, Osman et al. (2015) predicted crop types at the parcel level before the crop growing season using the first-order Markov chain on a four-year crop rotation pattern in southern France. However, Osman et al. (2015) used the frequency of crop rotation as a weight between states instead of transitional probability, which considers the long-term sequence.

In this study, CDL data from the past 11 years are used to develop the crop plantation sequence to predict crop types for the year of a flood event. We used transitional probability between crop types calculated from the sequence. Crop type in each year on a given field is a sequence of random variables $X_1, X_2, \dots, X_n, \dots$; and transitional probabilities between crop types are the degree of dependencies. Thus, the transitional probability (p_{ij}) from state s_i to state s_j is defined by Eq. 1.

$$p_{ij} = P_r(X_{n+1} = s_j | X_n = s_i) \quad (1)$$

A transition matrix of the probability of transitions from one state to another can be represented as $P = (p_{ij})_{i,j}$, where each element of position (i, j) represents the transitional probability p_{ij} . For instance if $r = 3$, a 3×3 transition matrix P is shown in Eq. 2.

$$P = \begin{bmatrix} p_{11} & p_{12} & p_{13} \\ p_{21} & p_{22} & p_{23} \\ p_{31} & p_{32} & p_{33} \end{bmatrix} \quad (2)$$

Figure 2 illustrates the detailed representation of Markov models for major crop rotation patterns by showing the Markov chain transitional probabilities for different sequences. An alternate pattern of crop rotation and their transitional probability for the next sequence is shown in Fig. 2a. In the corn-soybean alternate pattern, if the current state is corn, then the probability of soybean in the next state is 100% and vice versa. Therefore, the transitional probability from corn to soybean and soybean to corn is 1. Figure 2e shows a monocropping pattern of corn, which indicates the same crops every year. Therefore, the transitional probability of having the same crop is 1. Figure 2c shows a pattern where three crops are presented, the probabilities of transition from alfalfa to corn and soybean to corn are 1. However, the probabilities of transition from corn to soybean and corn to alfalfa are 0.6 and 0.4 respectively. Similarly, Fig. 2d and f show a more complex situation by including other crop types and noncropland covers. The lines with arrows show the direction of probabilities of transition from one state to another. In the case of a tie, prediction chooses one state randomly among states that have an equal chance.

2.3 Operational Flood Inundation Mapping Using Satellite Remote Sensing

Advanced Earth observation and geospatial technologies bring the opportunity to map flood inundation extents over vast areas very quickly. Moderate to coarse spatial resolution optical remote sensing systems (including MODIS, Visible Infrared Imaging Radiometer Suite (VIIRS), Landsat, and Sentinel-2) provide data with a higher temporal resolution, at frequencies from daily to every 2

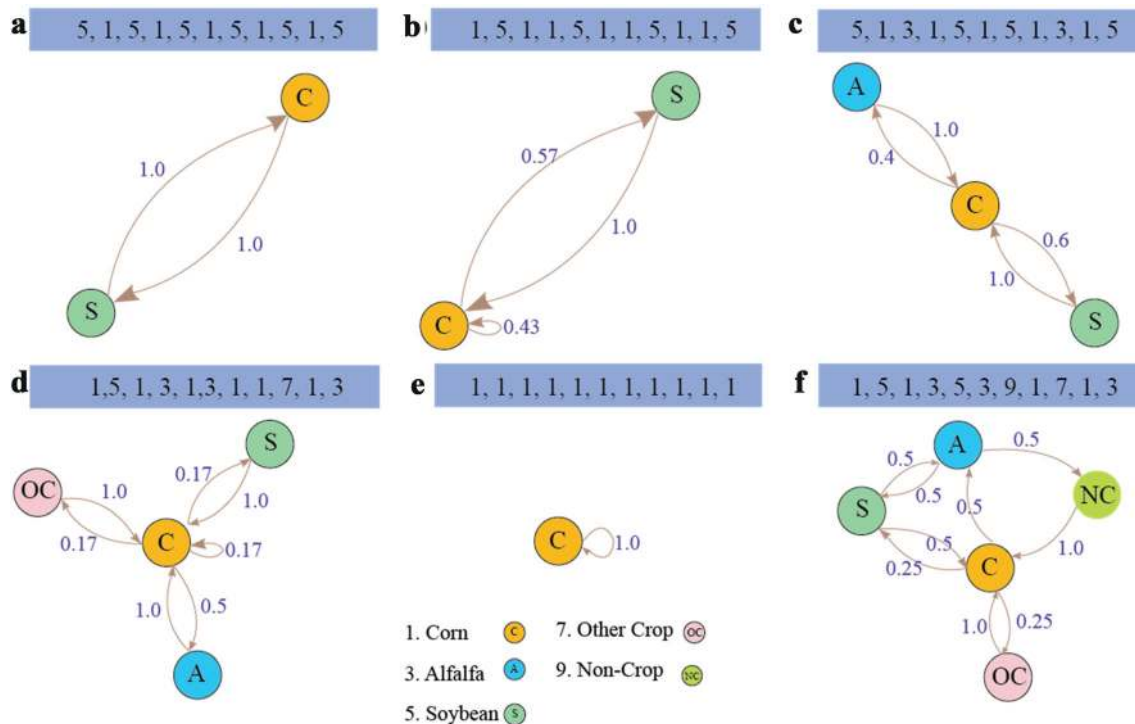


Fig. 2 Examples of Markov chains for major crop rotation patterns: **a** an alternate cropping pattern (soybean-corn-soybean) starting with soybean; **b** an alternate cropping pattern (corn-soybean-corn) starting with corn; **c** crop rotation pattern with three crops; **d** crop rotation

pattern with four crops; **e** mono cropping pattern with corn; **f** a complex crop rotation pattern with five types including four crop types and a non-crop land use

weeks. It is difficult to monitor flood progress in many cases because of the inability of optical remote sensing to see through clouds and canopies (Lin et al. 2016). It is equally difficult to detect storm-induced floods because of high cloud concentrations under low-pressure oceanic conditions. Hence, most of the optical remote sensing-based, flood monitoring systems are unable to provide flood inundation information during these cloud conditions. Microwave remote sensing, however, brings the opportunity for flood inundation mapping in all-weather conditions since microwaves can penetrate through clouds, aerosol, haze, and tree canopy. Although microwave remote sensing in flood mapping is becoming popular, data from most of the microwave remote sensing systems, especially Synthetic Aperture Radar (SAR), was not available free of charge before the launch of Sentinel-1. Thus, both optical and SAR options are explored with recent flood cases in Iowa, Nebraska, and Texas. Cloud-free Landsat images were not available for these selected case studies. Flood extents were mapped for Iowa and Nebraska cases using both Sentinel-1 (SAR) and Sentinel-2 (optical). Since these flood events were long, and satellites passed on different dates, both flood extent maps are combined to get the maximum flood extents. For the Texas event, flood extents were mapped using only Sentinel-1 data because of the

unavailability of cloud free optical data from Landsat and Sentinel-2.

2.3.1 Methodological Approach of Flood Mapping with Optical Remote Sensing

First pre- and post-flood event, cloud-free, remote sensing scenes are downloaded from data portals. The Modified Normalized Difference Water Index (MNDWI) is then calculated for both pre- and post-scenes using Eq. 3:

$$MNDWI = \frac{\rho_g - \rho_{mir}}{\rho_g + \rho_{mir}} \tag{3}$$

where ρ_g is the visible green band of Sentinel-2 MSI band 3. ρ_{mir} is a middle infrared band (MIR) of Sentinel-2 MSI band-8. The computation of MNDWI produces values between -1 and $+1$, where values greater than zero indicates water and values less than or equal to zero represent non-water pixels (Xu 2006). Although the threshold zero usually works for most of the cases, a threshold selection method from gray-level histograms proposed by Ostu (1979) is adapted to map water information. Pre- and post-event water information is then extracted from MNDWI maps using Ostu’s histogram thresholding approach. A change detection technique then is applied on

pre- and post-event water maps to map inundated areas, where each pixel is mapped as flooded if that pixel represents nonwater in the pre-event map and water in post-event map.

2.3.2 Methodological Approach of Flood Mapping with SAR Data

Similar to the optical remote sensing, pre- and post-flood water information derived from Sentinel-1 SAR data is compared to map flood inundation extent. Pre- and post-event Ground Range Detected (GRD) products are downloaded from the European Space Agency (ESA) Sentinel data portal. Vertical–Vertical (VV) polarization of Sentinel-1 data is used for the extraction of pre- and post-event water information because it is advantageous over Vertical–Horizontal (VH) cross-polarization considering the accuracy of flood mapping (Clement et al. 2018). The Sentinel Application Platform (SNAP) is used for calibration, range correction, speckle filtering, and binarization for preprocessing of the image, as well as to map water extents. Finally, histogram thresholding is used to separate water from land. The threshold is chosen based on the gray-level histograms thresholding approach proposed by Ostu (1979) for each scene. Subsequently, a change detection technique is used to extract flood information from pre- and post-flood water maps.

2.4 Methodological Process for the Degree of Crop Damage Assessment

This study combined flood information, in-field crop types, and crop condition profile for rapid crop damage assessment. Figure 3 illustrates a step by step workflow for rapid crop damage assessment. At first, MODIS daily NDVI data products are downloaded from a Web portal maintained by the Center for Spatial Information Science and Systems of George Mason University. Daily NDVI is calculated using MODIS daily surface reflectance L2G Global 250 m products (MOD09GQ and MYD09GQ). Equation 4, the mathematical expression of NDVI, is used to calculate NDVI from MODIS surface reflectance.

$$NDVI = \frac{\rho_{nir} - \rho_r}{\rho_{nir} + \rho_r} \quad (4)$$

where ρ_{nir} and ρ_r are surface reflectance in near-infrared (NIR) and visible red (VR) bands of the electromagnetic spectrum. The NDVI was calculated for the current flood year as well as for past years. After calculating NDVI, the median Vegetation Condition Index (mVCI) was calculated using Eq. 5. The daily mVCI of the current year and past years are calculated from daily NDVI. All mVCI maps between 2000 and the year before the year of

flood event are considered as the historical mVCI. Therefore, $NDVI_{\max(x,y)}$, $NDVI_{\text{med}(x,y)}$, and $NDVI_{\min(x,y)}$ at a pixel (x,y) are the maximum, median, and minimum of the historical time series. To calculate mVCI before and after a flood event, two windows are considered to take cloud-free mVCI data. Since clouds may exist over a longer period of time before a flood event, a 14-day long window before flood events is chosen to get useful mVCI. Similarly, a short 7-day window is chosen to calculate mVCI after flood events. A shorter after-event window is chosen to avoid the potential contamination of grass and weed in cropland.

$$mVCI = \frac{NDVI_{(x,y)} - NDVI_{\text{med}(x,y)}}{NDVI_{\max(x,y)} - NDVI_{\text{med}(x,y)}} \quad (5)$$

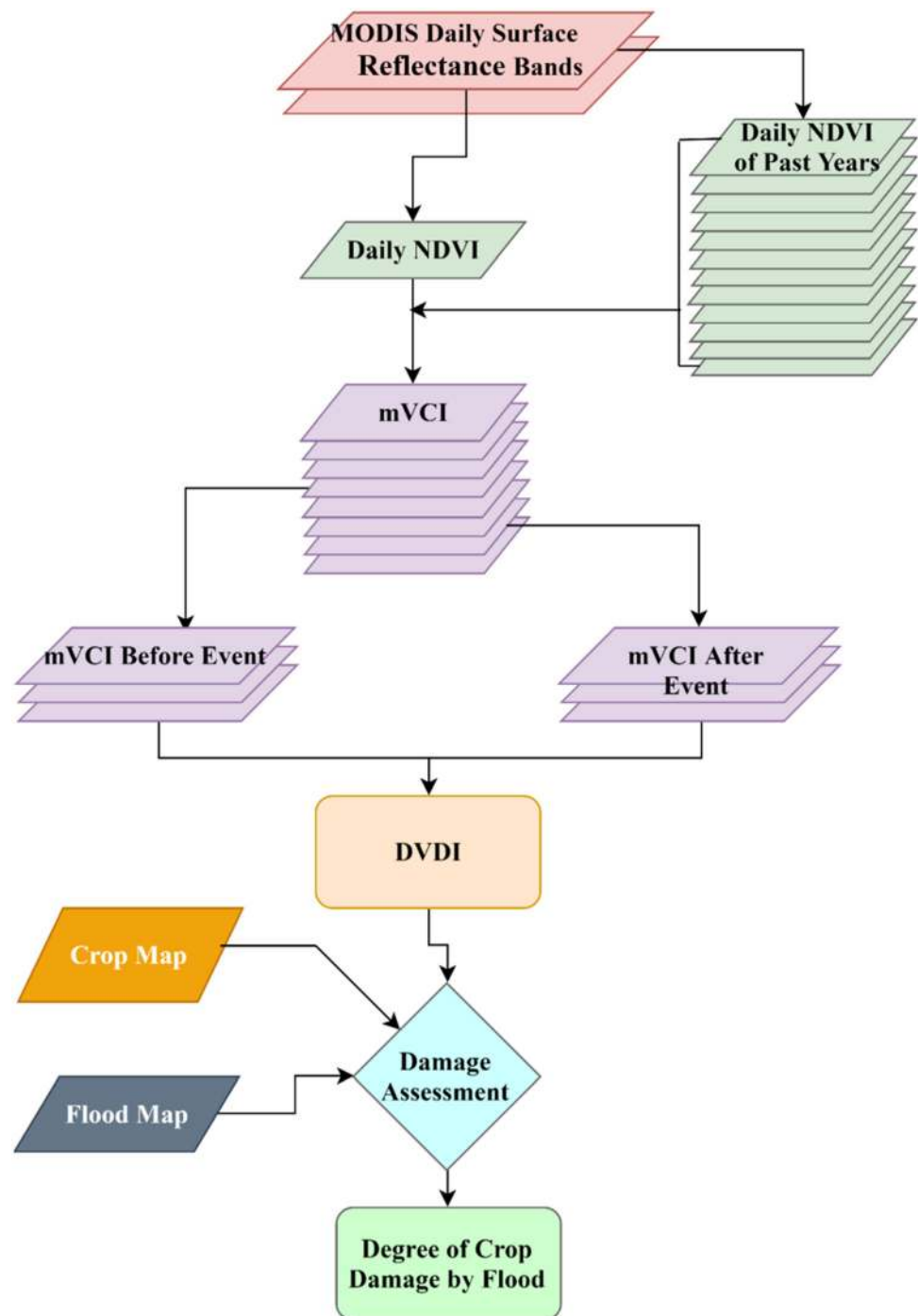
After calculating pre- and post-event mVCI, DVDI was calculated by taking the difference between pre- and post-event mVCI. The mathematical expression of the DVDI index is given in Eq. 6.

$$DVDI = mVCI_a - mVCI_b \quad (6)$$

where $mVCI_a$ and $mVCI_b$ are the vegetation conditions immediately after and before a disaster respectively. A positive DVDI indicates no damage and a negative value indicates considerable damage to the vegetation. Since the possible values of DVDI are inherited from NDVI, the range of DVDI value is also between -1 and $+1$. Crop NDVI may change for several reasons, such as pest attack and crop phenological change. Thus, DVDI only considers the change immediately before and after the event to reduce the impact of other changes in crop profiles. The underlying assumption is that crop profile changes between immediately before and after flood events only because of flood impact. Moreover, NDVI varies across the days of the year because of seasonal change. Therefore, any comparison of NDVI should be specific to the day of year and location. Each mVCI was calculated by comparing NDVI with the historical median NDVI of the same day of the year (DoY).

Since the goal of this research is to find flood crop loss, DVDI maps are masked by combined flood inundation extents derived from operational flood mapping that uses both optical and SAR data. The DVDI of flooded areas is then masked by crop areas to map the degree of crop-specific damage. Three different maps are derived from images of different spatial resolutions: Flood extents derived from 10 m sentinel data; DVDI derived from 250 m MODIS data; and crop types are mapped at 30 m CDL spatial resolution. All maps are resampled to 10 m for the suitability of the analysis. The continuous variable DVDI can be categorized into a subjective scale of the degree of damage by using the different ranges of negative values (Di, Yu et al. 2018). Many case studies also divided

Fig. 3 The methodological framework for crop-specific flood loss assessment from MODIS surface reflectance bands



crop damage into four to six categories using subjective scales (Okamoto et al. 1998; Islam and Sado 2000; Capellades et al. 2009; Chowdhury and Hassan 2017). This is, in fact, a very common approach for the reporting of rapid crop damage. In this study, the degree of damage is categorized into six classes: No damage, very slight damage, slight damage, moderate damage, severe damage, and very severe damage. The positive values (≥ 0) of DVDI

are labeled as “No Damage.” Negative values of DVDI are categorized into five ordinal classes using equal intervals. These five categories are defined as $0 > DVDI \geq -0.1$: “Very Slight Damage”; $-0.1 > DVDI \geq -0.2$: “Slight Damage”; $-0.2 > DVDI \geq -0.3$: “Moderate Damage”; $-0.3 > DVDI \geq -0.4$: “Severe Damage”; $-0.4 > DVDI$: “Very Severe Damage.”

2.5 Damage Assessment Validation Process

It is important to validate the loss assessment model with actual flood damage on crops. Plot-level crop yield loss information could be the best option for model validation. But plot-level information on crop yield loss is not available publicly. Public access to these crop loss databases is restricted because of the location information and personal information associated with it (Shrestha 2017). Our research utilizes two approaches for the validation of crop damage assessment. First, the visual assessment is conducted by comparing NDVI curves of different damage categories. Since NDVI has a strong positive correlation with crop yield, a significant drop in the NDVI curve is the indication of crop damage (Shrestha et al. 2016; Ahmed et al. 2017; Shrestha et al. 2017). Second, the relationship between the loss percentage of crop yield and DVDI values can be used for validation. Positive DVDI corresponds to no loss and negative values indicate crop damage; whereas smaller values are the indication of higher loss.

2.5.1 Pixel-Level Validation

Three hundred sampling locations are generated using the equalized stratified random sampling technique for each case study. Since there are six damage classes, 50 points are taken for each class. Figure 4 shows the spatial locations of sampling points. After determining the sampling locations, the daily NDVI time series data are extracted at sampling locations for the corresponding years of flood events. Then NDVI time series are obtained from 2018 for the Iowa flood event and the Nebraska flood event. Similarly, the NDVI time series for the Texas flood event is extracted from the 2016 NDVI data.

Since NDVI is obtained from optical remote sensing bands of MODIS, the daily NDVI is often contaminated by atmospheric conditions such as cloud, haze, and dust. Thus, this study used a two-level filtering approach of NDVI noise removal that employed the Best Index Slop Extraction (BISE) and Savitzky-Golay filter. The performance of the Savitzky-Golay filter is better than other selected approaches for the noise removal of the NDVI time series (Rahman et al. 2016). Rahman et al. (2016) provide a detailed methodological process that achieves noise reduction from the MODIS derived NDVI profile of crops. A total of 300 smoothed NDVI curves are obtained for each case study after removing noise. A generalized NDVI curve is then constructed for each damage category by taking an average of 50 NDVI profiles that corresponds to the specific class. Finally, the six generalized NDVI curves of the different degree of damages are plotted against day of year for the comparison among damage categories for each case study.

2.5.2 Plot-Level Validation

The plot-level validation of damage assessment is conducted by the relationship between yield loss and DVDI values. Since direct crop loss data are not available from the public domain, our research calculated crop yield loss by comparing the yield of the affected year with a previous year yield at the same plot location. Since plot-level yield data are not available from the portal of the USDA National Agricultural Statistics Service (USDA-NASS), we acquired yield data alternatively from the portals of various seedling companies. Seed companies provide some plot-level yield data from locations where farmers planted the companies' seed variety. Yield information was collected

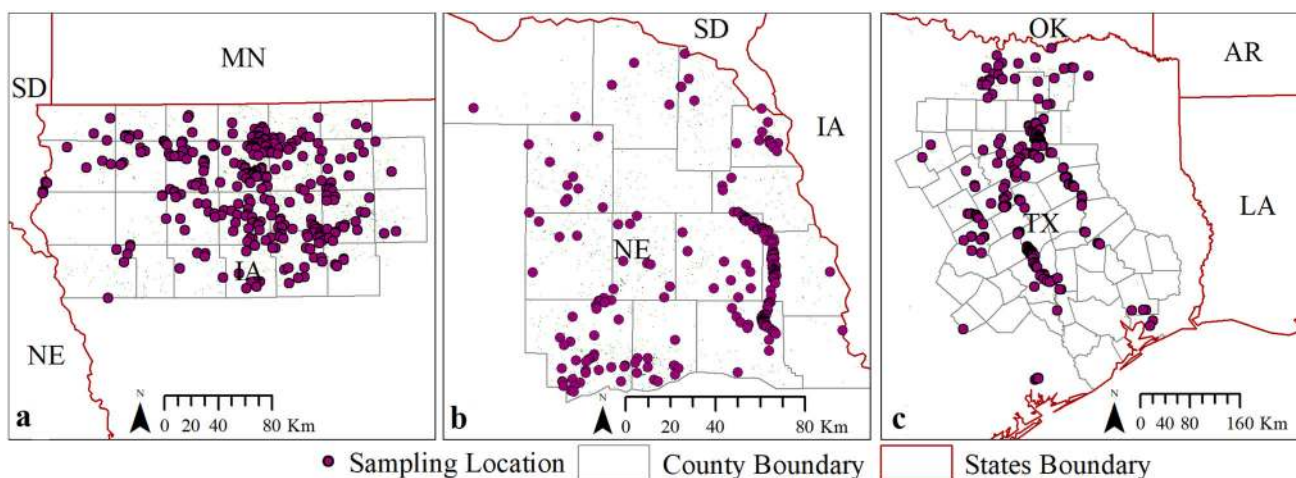


Fig. 4 Sampling point locations of pixel-level validation. **a** the Iowa flood event in 2018; **b** the Nebraska flood event in 2018; and **c** the Texas flood event in 2016

from five major companies including Pioneer Hi-Bred International, Beck's, Syngenta, Bayer Global, and Golden Harvest Seeds for their coverage in the selected study areas.

It is important to select those plots that have data on the same crops for the current year and the past year. Therefore, this searching process only includes these plots that are in flood-affected areas and have data on the same crops in a flooded year as well as in some of the past years. Although all five source portals of seed companies provide an embedded base map on their website, it is not possible to extract geographic coordinates of plots from these portals. Thus, Google Maps is used as an auxiliary reference source to identify plot locations by cross-referencing them with embedded maps in these data portals. The targeted plot is visually identified in both the embedded map and Google Maps using the crossing point of nearby roads. If the embedded map has an image view, the process is easier to match with the Google Maps image view.

Figure 5a illustrates an example of a corn yield plot location in Iowa in the data portal of Bayer Global. Figure 5b shows the location of the same plot in Google Maps. The left panels of Fig. 5a show the corn yield information of the same plot in 2017 and 2018. Once a targeted plot is correctly identified in Google Maps, geographic coordinates are extracted using pinpoint of Google Earth. Yield information of the corresponding plot is also stored in an excel database. This process is repeated for each available plot from these data portals. A total of 37 suitable plots were found for plot level validation.

After completing the database for all selected plots, a GIS database is created from the excel database using the coordinates of these plot locations. This GIS database is then projected to the USA Contiguous Albers Equal Area Conic projection system. These coordinates are used further to acquire the corresponding plot-level DVDI, the center pixel of which usually is considered for the representation of the plot. Yield loss of these plots is calculated in percentage by taking the ratio of yield loss to the yield in any previous year. Here, the loss is defined as the subtraction of yield in the past from the yield of the flood-affected year. Figure 6 illustrates the location of selected plots for the validation, where yellow and green color indicates the location of corn and soybean fields, respectively.

3 Results

The result section illustrates the significance and accuracy of the crop type mapping using Markov chain modeling in Sect. 3.1. Then crop damage assessment results from the three case studies are discussed in the following

subsections. Finally, Sect. 3.3 shows the validation of crop damage assessment results.

3.1 Prediction of Field-Level Crop Type Results

The predicted field-level crop types are compared with USDA CDL data for the corresponding year of flooding events. The predicted crop type maps are very similar to CDL. The accuracy of crop type prediction is assessed for Iowa through spatial agreements with CDL and ground truth data. A total of 100,000 pixels are selected over croplands using stratified random sampling to assess the spatial agreement with CDL. The predicted map has an overall agreement of 87% with CDL. The kappa value 0.80 also indicates a higher spatial agreement with CDL. Corn has the highest producer agreement (85%) among all crop types. Soybean has 82% user agreement and 73% producer agreement. Although very high agreement can be achieved for corn and soybean, prediction accuracy is low for other crops such as wheat, rye, oats, and alfalfa. The reason for the low prediction accuracy for these crop types is inconsistent and insufficient rotation pattern. The prediction model needs to be learned from sufficient number of plots of consistent rotation pattern for accurate prediction.

Similarly, the accuracy of crop type prediction is assessed through 678 ground truth samples for Iowa collected from the field visit during the crop growing season in 2018 (Rahman et al. 2019). The sampling was used to collect these ground truth data along major highways in the southwestern, northern, southeastern, and central parts of Iowa. Geotagged photos of crop fields were collected using cellphone device (iPhone 7). Finally, ground truth data were prepared using photo interpretation and extraction of location information from geotagged photos. The result shows 85% prediction accuracy with a kappa value of 0.69. The prediction accuracy for corn is very high, where user accuracy and producer accuracy are reported at 91% and 93% respectively. Soybean also shows high user accuracy (82%) and producer accuracy (79%). Alfalfa shows reasonable prediction accuracy (75% user accuracy and 64% producer accuracy). The high spatial agreement and accuracy are probably achieved in corn and soybean prediction because of the stable crop rotation patterns of these two major crops.

3.2 The Rapid Assessment of Flood Crop Damage

Flood crop damage is assessed for three selected case studies. The assessment results are discussed for Iowa, Nebraska, and Texas as case studies 1, 2, and 3, respectively in the following.

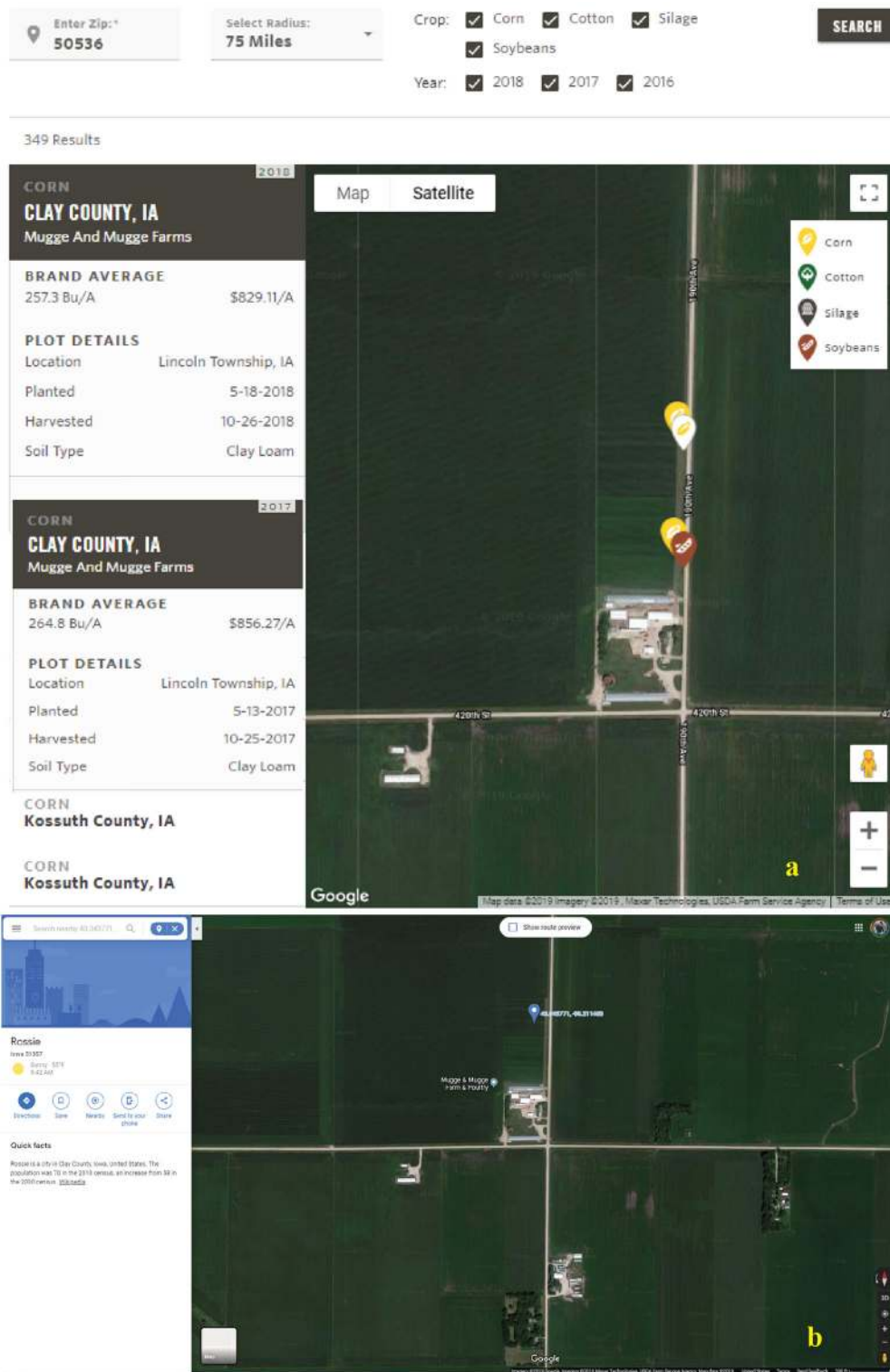


Fig. 5 Sampling point locations of pixel-level validation. **a** Satellite view of plot location in the portal of Bayer Global; **b** Image view of the same location in Google Maps

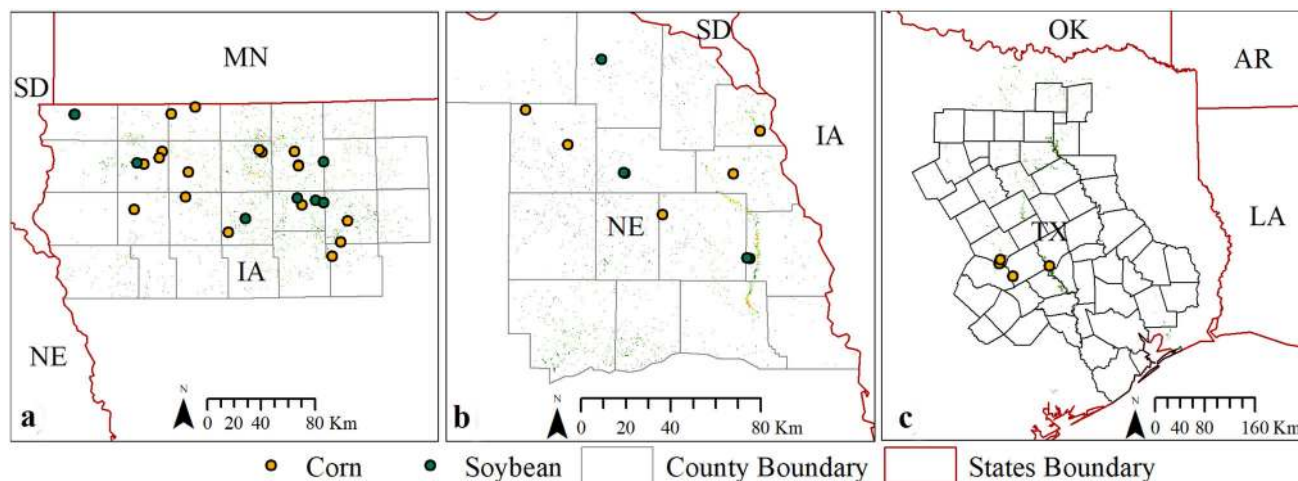


Fig. 6 Sampling point locations of pixel-level validation. **a** the Iowa flood case; **b** the Nebraska flood case; **c** the Texas flood case

3.2.1 Case Study 1: Iowa Severe Storms and Flooding (DR 4386)

The incident period of the Iowa Severe Storms and Flooding event was between 6 June and 2 July in 2018, which indicates the flood event occurred in the greening and maturing stage of major crops in Iowa. Figure 7 illustrates the pixel-level degree of vegetation damage in the northwestern part of Iowa. Four zoomed-in panels show the degree of crop damage in four randomly selected locations within the affected areas. Although many crop fields were flooded, the dark green colors indicate no damage by the floods (Fig. 7a, b, d). Many croplands are severely damaged on both sides of the Des Moines River (Fig. 7c). The duration of floods may be one of the reasons for the different degrees of damage in crop fields.

Figure 8 provides quantitative measures of damage to major crops in six selected counties in Iowa. Only three crops of corn, soybean, and alfalfa are considered for damage assessment because of the negligible presence of other crop types in Iowa. Four counties show soybeans having higher acreage of severe to slight damage (Fig. 8a–d). In contrast, most of the flooded cornfields have no or slight damage in all selected counties. Corn is usually taller than soybean, which could be the cause for higher damage in soybean compared to corn.

A total of 153 ha of soybean faced moderate to very severe damage in Osceola County. More than 60% of flooded cornfields have no damage in Osceola (Fig. 8a). Similarly, almost half of flooded corn has no damage whereas 60% of affected soybean has a higher degree of loss in Kossuth (Fig. 8b). Clay is one of the most affected counties, where 174 ha of corn and 237 ha of soybeans are severely damaged. An additional 262 ha of corn and soybean are moderately damaged in this county (Fig. 8c).

Figure 8b and d show almost similar crop damage patterns in Palo Alto and Kossuth. A few hectares of alfalfa have slight to moderate damage in most of the selected counties. Both corn and soybean have mostly slight to moderate damage in Humboldt and Wright Counties (Figs. 8e and f).

3.2.2 Case Study 2: Nebraska Severe Storms and Flooding (DR 4387)

Similar to the flood event in Iowa, the Nebraska Severe Storms and Flooding event also occurred in June 2018. Most of the affected counties are adjacent to the affected counties in Iowa. Thus, these two flood events are mostly the result of a severe storm in June over Nebraska and Iowa. Figure 9a–d show four detailed views of the degree of damage of flooded croplands taken from four locations in the affected regions. Croplands in some counties, such as Dixon, Dakota, Thurston, and Cuming, are severely affected. Panels 9b and 9c show severe damage in most of the flood-affected croplands. Panel 9a from Platte County shows no damage or slight damage in most of the affected croplands.

Figure 10 illustrates the quantitative assessment of the different degrees of crop damage in six selected counties. Most of the affected crop fields have no or slight damage in Dixon County. Only around 6 ha of soybean has moderate to severe damage. More than half of the affected soybean has slight to moderate damage and negligible severe damage in Dakota County. Although corn has very negligible damage, nearly 150 ha of soybean has moderate to severe damage in Thurston. Cuming is the most affected county where nearly 350 ha of soybean has moderate to severe damage; more than 400 ha of soybean experienced slight damage. There is almost no damage in affected croplands in Colfax and Wayne Counties. The damage in

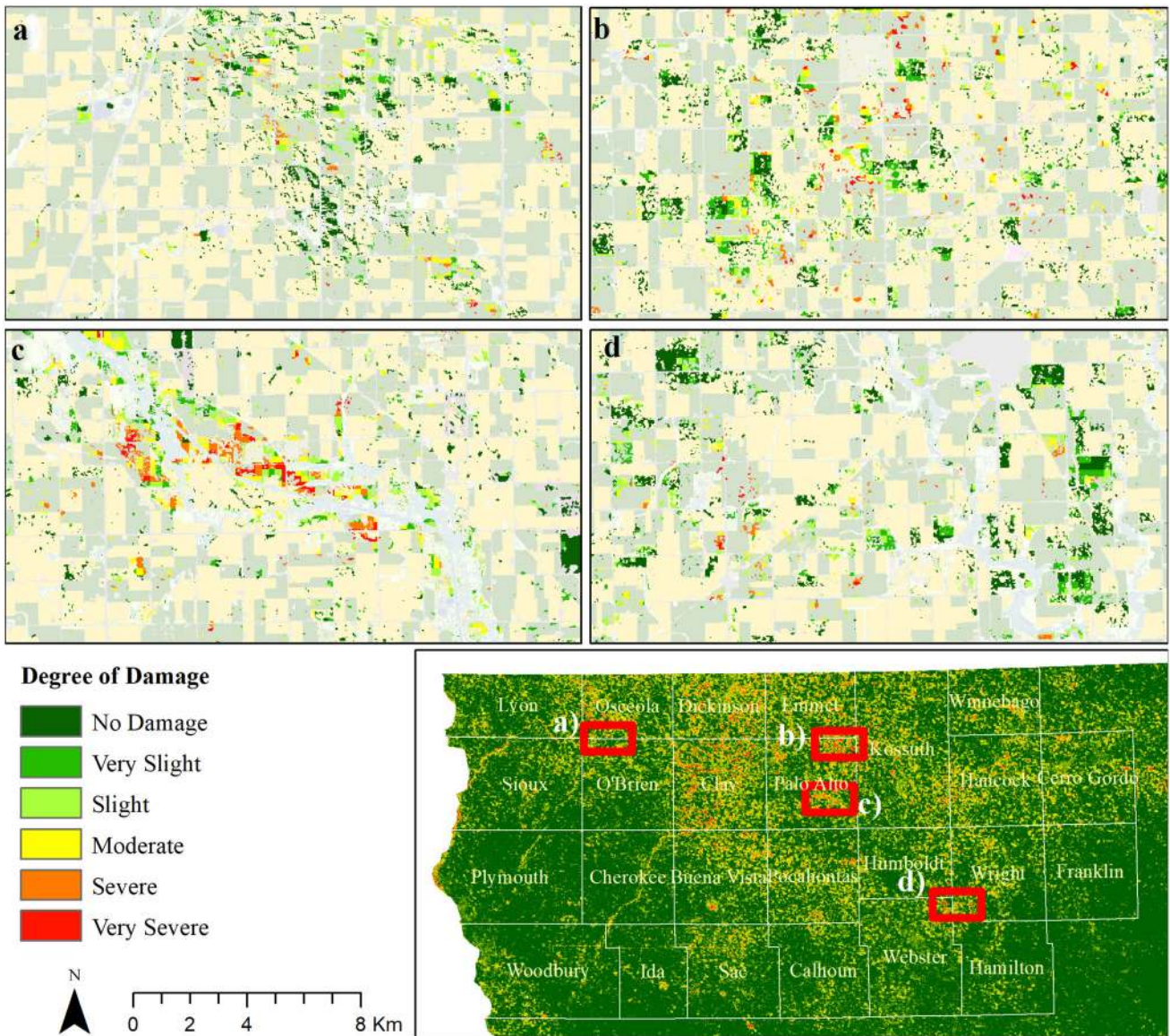


Fig. 7 The degree of damage of flood-affected croplands during the 6 June to 2 July Iowa Flood in 2018: **a** southwestern Osceola & northwestern O’Brien Counties; **b** northeastern Palo Alto County;

c southeastern Palo Alto County; and **d** northeastern Webster & southwestern Wright Counties

alfalfa fields is also very negligible in flood-affected counties in Nebraska.

3.2.3 Case Study 3: May 2016 Texas Flood

The Texas flood event occurred between 22 May and 24 June 2016, and impacted more than 20 counties. Figure 11 shows the degree of crop damage in flood-affected counties. The zoomed-in view of four locations is also shown in Panels a–d. Similar to other case studies, no damage and slight damage are also more frequent compared to severe damage.

Figure 12 illustrates the damage to different crop types in four selected counties. Unlike Iowa and Nebraska, cotton, sorghum, and oats are also major crops along with corn, soybean, and alfalfa in Texas. Many croplands have winter wheat in Texas. Corn is severely affected in Anderson County where moderate, severe, and very severe damage are accounted for 284, 260, and 194 ha respectively. There was no damage to soybean and oats in Anderson County (Fig. 12c). Alfalfa is the most affected crop type in Navarro County. More than 200 ha of alfalfa have moderate to severe damage, and more than 600 ha are slightly damaged (Fig. 12b). Nearly 300 ha of soybean are

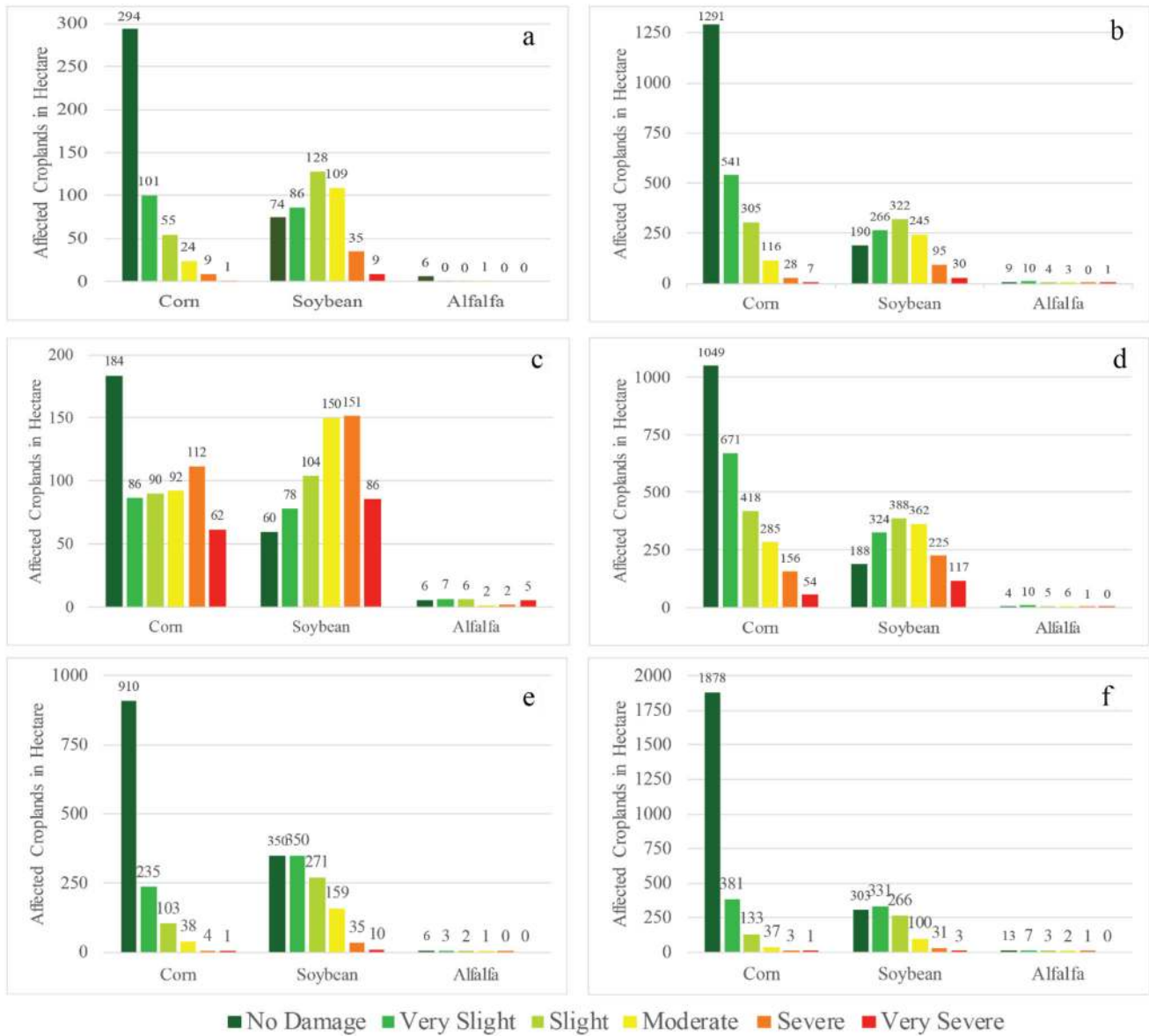


Fig. 8 The quantitative assessment of damage on major crop types in six selected counties in Iowa: **a** Osceola; **b** Kossuth; **c** Clay; **d** Palo Alto; **e** Humboldt; **f** Wright

moderately to severely damaged in Ellis County (Fig. 12a). Cotton is the most affected crop in Robertson County where about 1000 ha of cotton have slight to moderate damage. It is also observed that major crop types vary significantly from county to county in Texas.

3.3 Validation of Damage Assessment Result

Damage assessment results are validated using two different approaches: pixel-level validation by comparing NDVI profile and plot-level validation using yield loss information. These validation results are discussed below.

3.3.1 Pixel-Level Validation

The result of the pixel level validation is presented through the average daily NDVI profile of each damage class. Figure 13 illustrates the average NDVI curve for each damage class for the three case studies. Subplots a, b, and c, in Fig. 13 represent the average daily NDVI profile of damage classes for the Iowa, Nebraska, and Texas flood cases, respectively. Red, orange, yellow, light-green, green, and dark-green color indicates the NDVI profile for the damage classes—very severe, severe, moderate, slight, very slight, and no damage, respectively. Two vertical

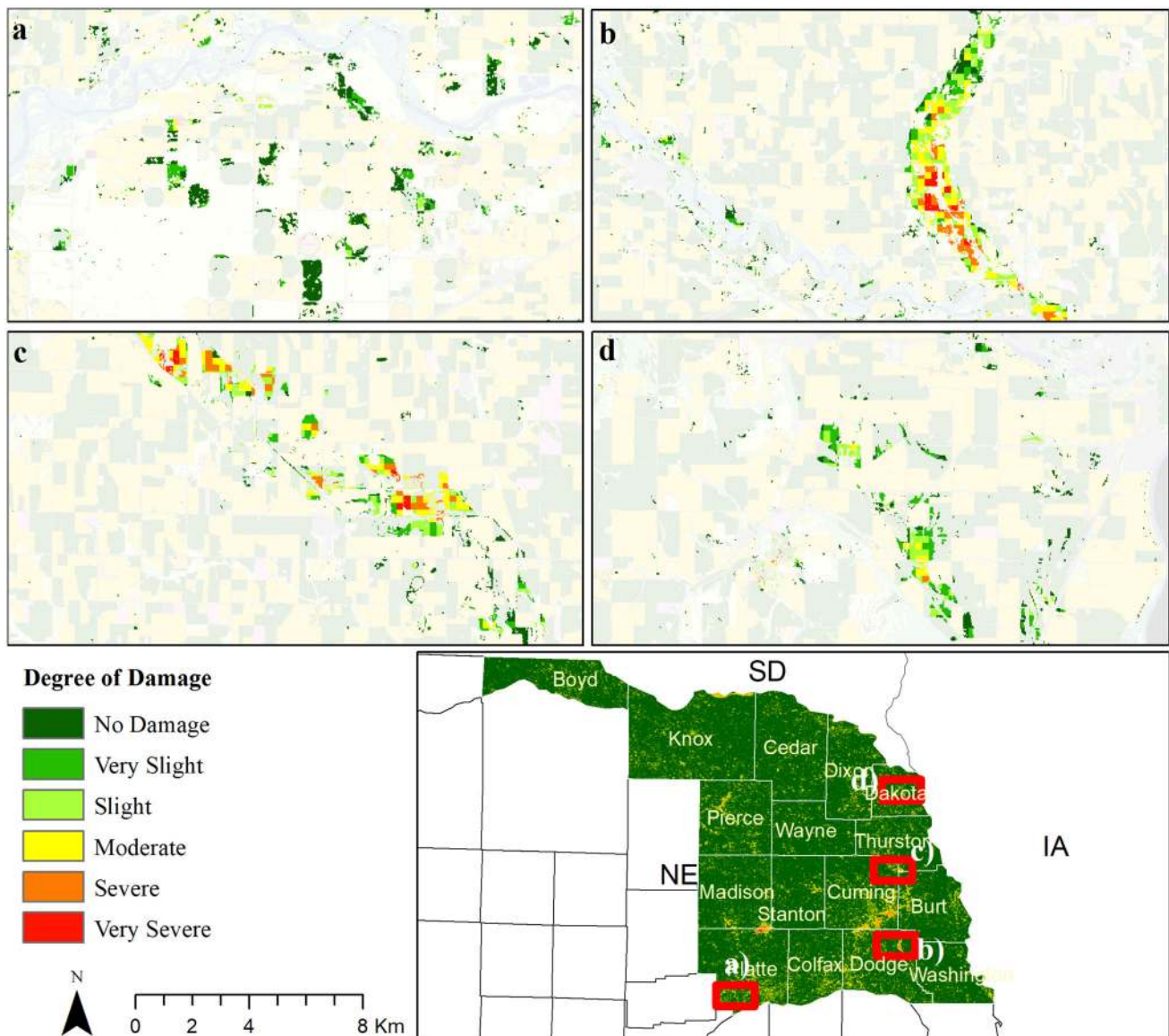


Fig. 9 The degree of damage of flood-affected croplands during the 17 June to 1 July Nebraska flood in 2018: **a** Platte County; **b** Dodge County; **c** Cuming County; **d** Dakota County

dotted lines indicate the start and end date of the flood events, respectively. There is a clear drop in NDVI values after a flood event for different damage classes. The deviation of the NDVI curve of different damage categories compared to the curve of the no damage category is the indication of the degree of damage.

As expected, the red lines of the very severe damage class show the highest drop in the NDVI profile after flood events. The orange lines of severe damage indicate the higher deviation after red lines. Similarly, other curve lines of damage classes also show considerable deviation from the NDVI curve of the no damage class, although the shape of the curve of each flood case is different from each other depending on many factors such as event duration and crop phenology during the event. Figure 13c shows a huge drop

in and a right shift of the red line, which may indicate crop replantation after having a total loss at the beginning of the growing season. Although Fig. 13a and b do not show a clear drop in the NDVI profile during the event, the impact is clearly visible after 2–3 weeks of the event. This is probably because the crop phenology stage is different in Nebraska and Iowa compared to Texas. The shape of NDVI curves looks similar in Iowa and Nebraska, probably due to the domination of similar crop types and crop phenology stage.

3.3.2 Plot-Level Validation

The yield information of a crop for multiple years is available only for 37 plots from all three flood cases. A

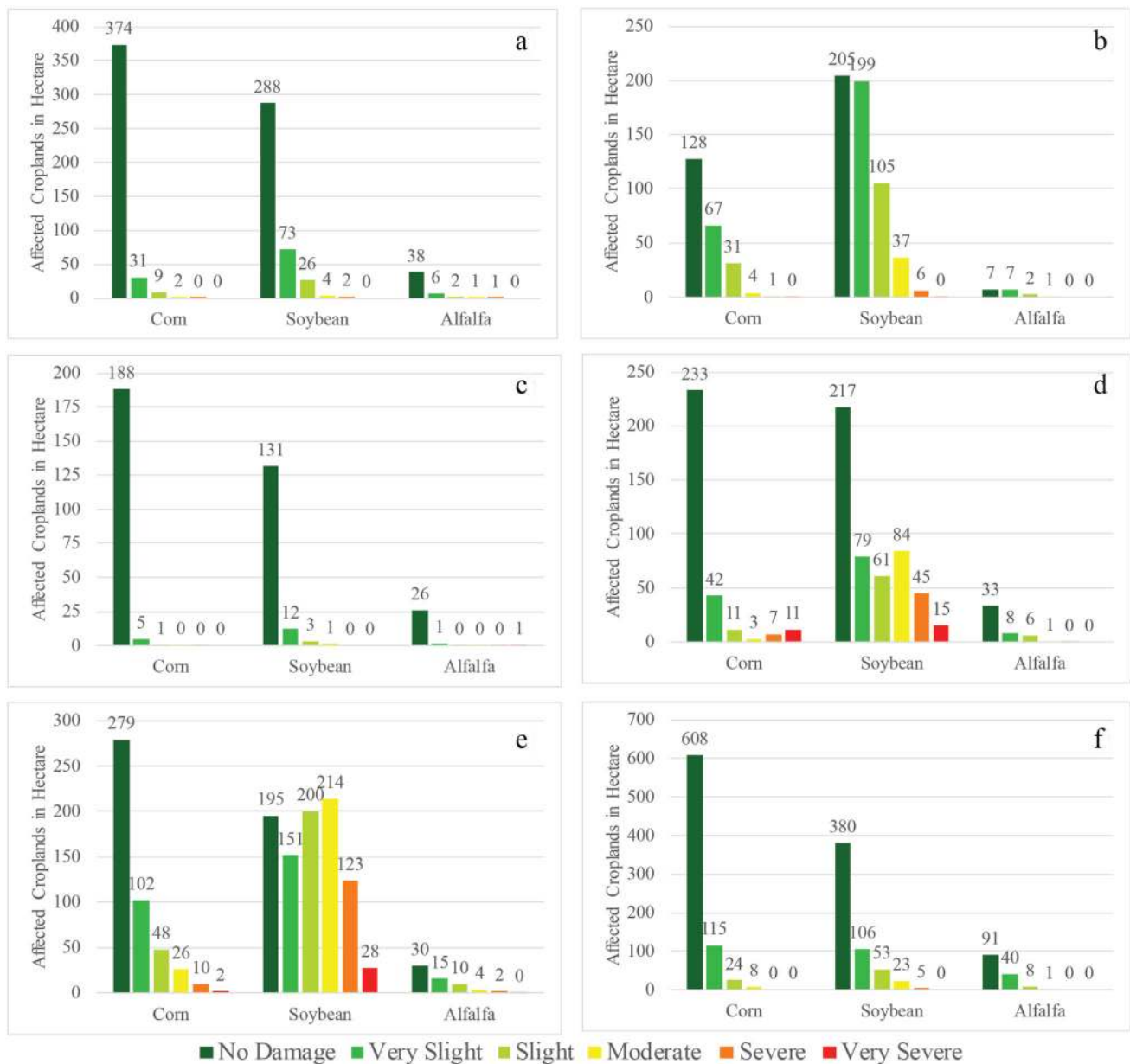


Fig. 10 The quantitative assessment of damage on major crop types in six selected counties in eastern Nebraska: **a** Dixon; **b** Dakota; **c** Wayne; **d** Thurston; **e** Cuming; **f** Colfax

total of 23, 10, and 4 plots are available from the Iowa, Nebraska, and Texas flood cases respectively. The percentage yield loss and corresponding DVDI values are plotted in Fig. 14. The positive values in yield loss are the indication of no loss.

The higher negative values should correspond to higher crop loss and vice versa. Among the 14 sampled plots with positive DVDI value, 11 plots correspond to positive yield loss (no loss). A total of 23 plots have negative DVDI, all of them also corresponding to yield loss. Therefore, it can be concluded that DVDI values can successfully indicate crop loss. Although low R^2 (0.5441) value indicates that a

relationship between DVDI and percentage yield loss is not particularly strong, the overall indication of crop loss can be made using the DVDI index.

Table 1 shows another evaluation of the damage category through percentage yield loss. Among the 14 plots of no damage category, 11 plots have no loss. Only 3 plots of the no damage category have less than 10% crop loss. Eight out of the 15 plots of very slight damage category have a yield loss of less than 10%. Half of the plots in the slight damage category have less than 10% loss and the other half belong to the group of 10–20% yield loss. Two plots of moderate damage category have 10–20% loss and

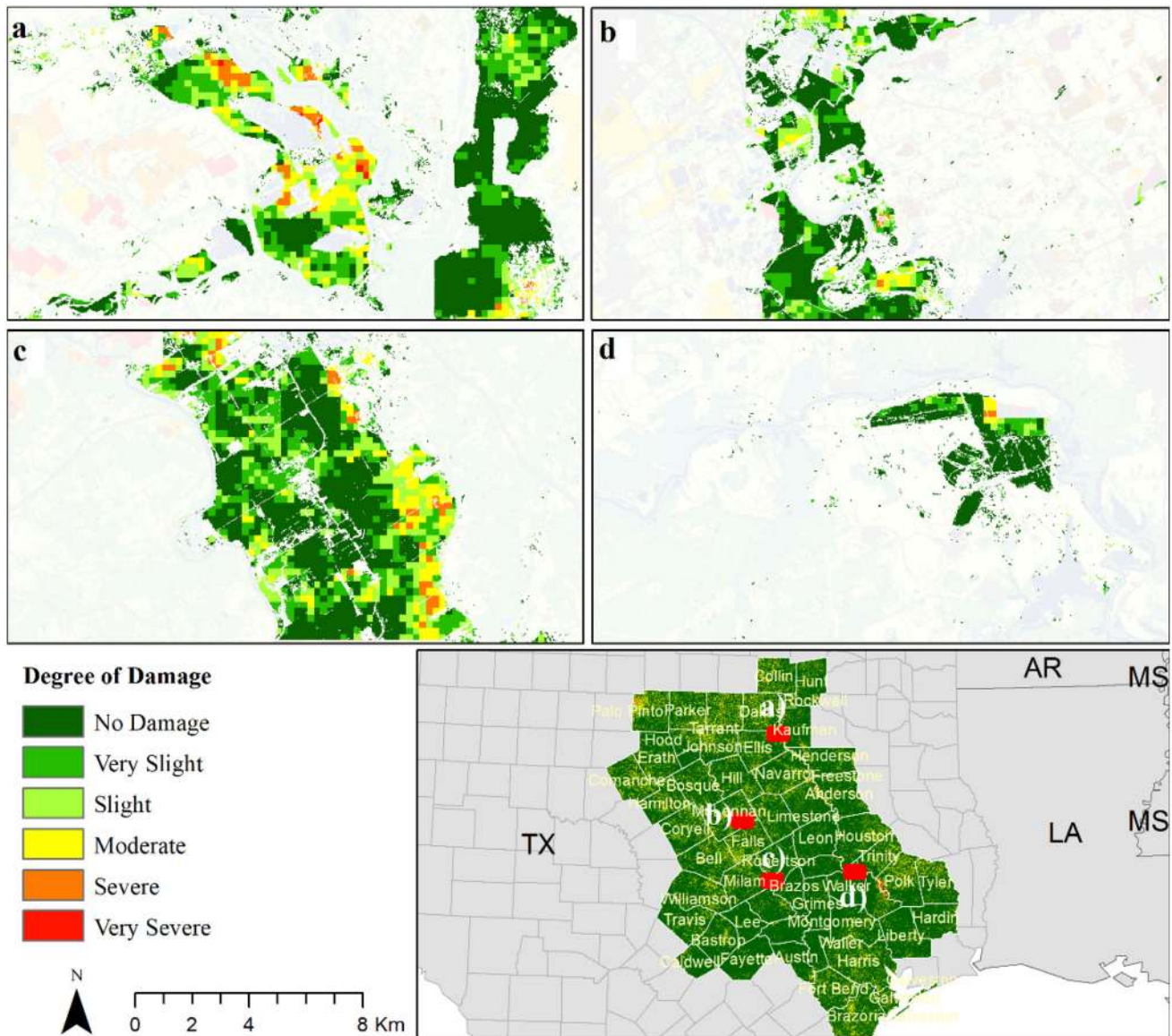


Fig. 11 The degree of damage of flood-affected croplands during the Texas Flood in 22 May to 24 June in 2016

only one plot has a 30–40% loss. Only one plot is in the severe damage category, which corresponds to about 48% loss.

4 Conclusion

A newly developed index called DVDI (Disaster Vegetation Damage Index) is used in this study to assess the flood impact on crops for three selected case studies in Iowa, Nebraska, and Texas. Five crop damage classes—very slight damage, slight damage, moderate damage, severe damage, and very severe damage—are defined to express the degree of damage using some equal interval ranges of negative DVDI values. DVDI maps are masked by the

areas of inundated croplands to get crop damage caused only by flood events. The degree of damage is also validated in two ways: (1) NDVI profiles of damage classes are compared to see the potential drop in NDVI compares to the no damage curve; and (2) evaluate the relation of DVDI with crop yield loss.

Crop-specific damage levels at the county scale are also calculated for selected counties as representative examples. The results show that many croplands were inundated during flood events, but no damage occurred. Croplands in some counties have moderate to severe damage. Very severe damage occurred only in a few croplands in most of the cases. The results also indicate that soybean fields had higher damage compared to corn in most of the counties in Iowa and Nebraska, probably because corn stalks are taller

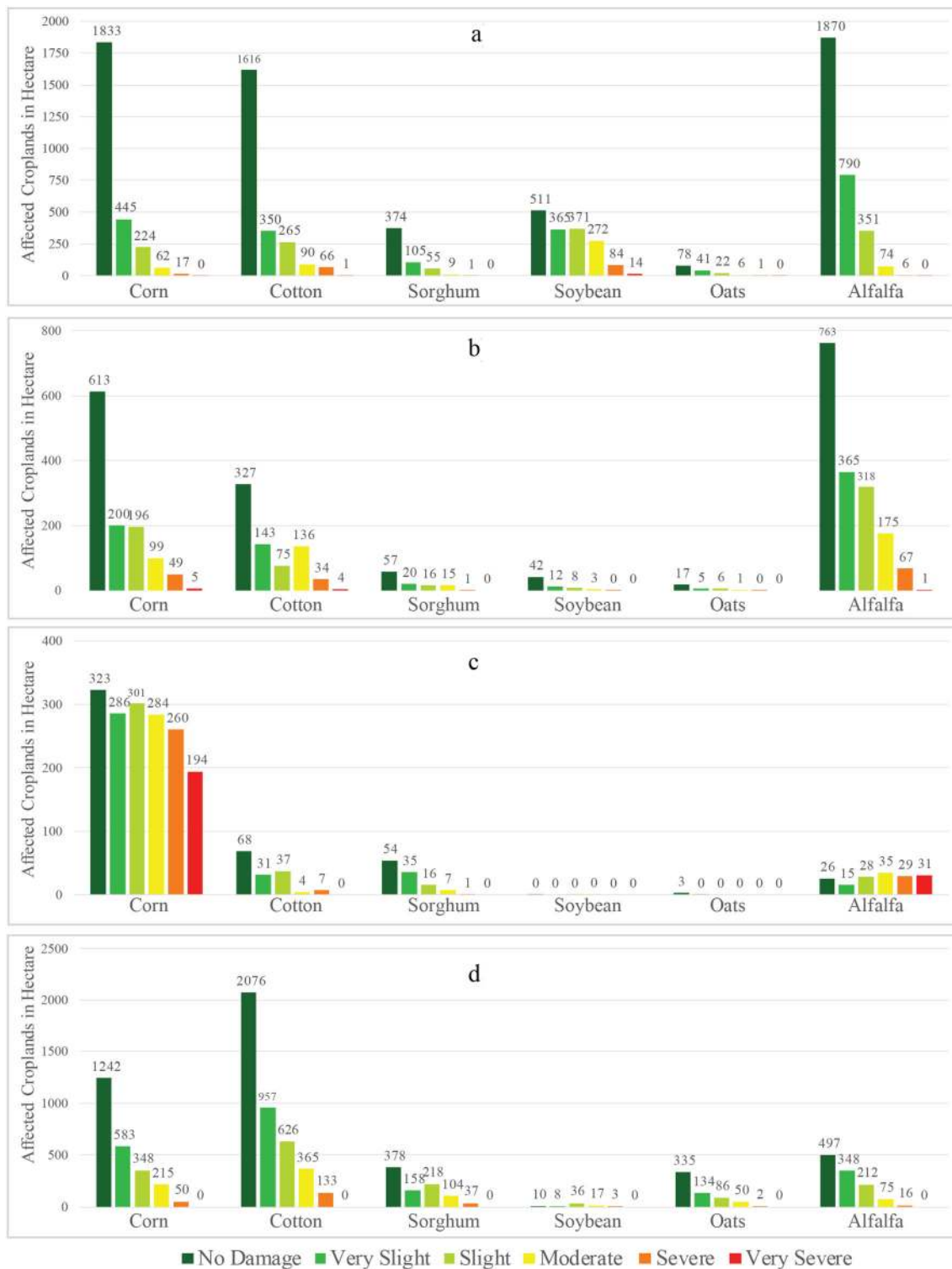


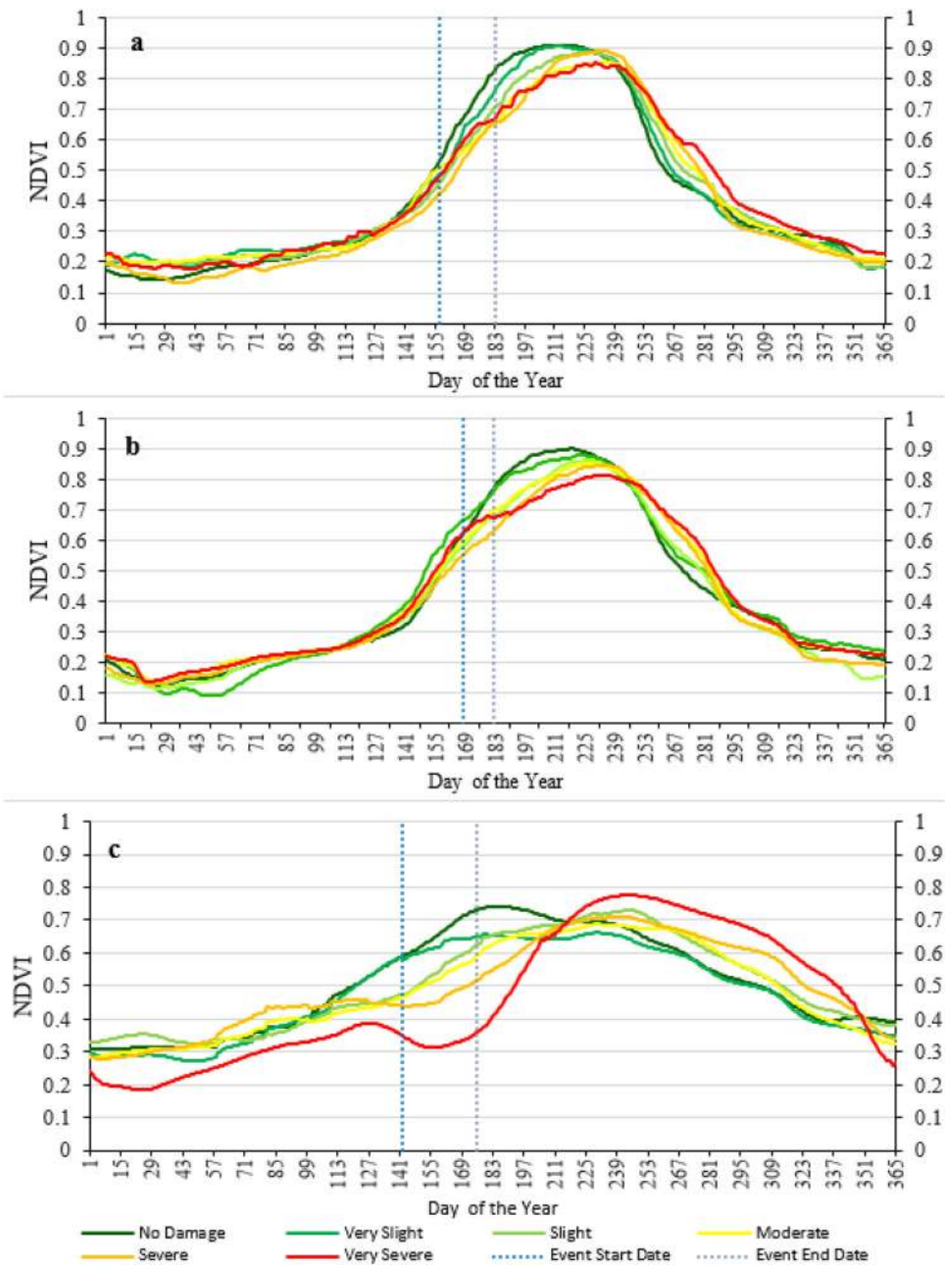
Fig. 12 The quantitative assessment of damage on major crop types in four selected counties in eastern Texas: **a** Ellis; **b** Navarro; **c** Anderson; **d** Robertson

than soybeans. The validation results indicate a strong relationship between DVDI and yield loss. The results also show that damage classes correspond to the drop in the NDVI profiles. Thus, it can be concluded that the degree of

damage can be explained using a DVDI-based qualitative scale.

Although DVDI-based qualitative assessment can be used in rapid crop damage assessment, there are some

Fig. 13 Comparison among the NDVI curves of different damage classes in **a** Iowa; **b** Nebraska; and **c** Texas



limitations and constraints in this process. There were significant differences in flood damage among counties affected by the same flood event. The possible reasons could be flood depth, crop types, and phenological difference. Since this research did not include flood depth information in the process, it is difficult to conclude the exact reason for the difference in crop damage. The ranges of negative DVDI may need to be adjusted to convert it on a subjective scale for different geographic contexts as well as for different crop types. The length of a window for mVCI selection before and after flood events needs to be carefully chosen, since outcome is sensitive to the selection

of windows. The choice of windows also depends on the objective of whether the assessment process captures the instant effect of events or captures the condition of the recovered crop. Moreover, cloud contaminated pixels need to be carefully excluded from daily mVCI. There are also important uncertainties in both remote sensing-based flood mapping and crop mapping. Flood mapping with Earth observation data results in underestimation or overestimation rather than actual flood extent dimensions. Similarly, the error in crop mapping may affect the accuracy of crop-specific damage assessment. Validation is always challenging because plot-level correct loss information is

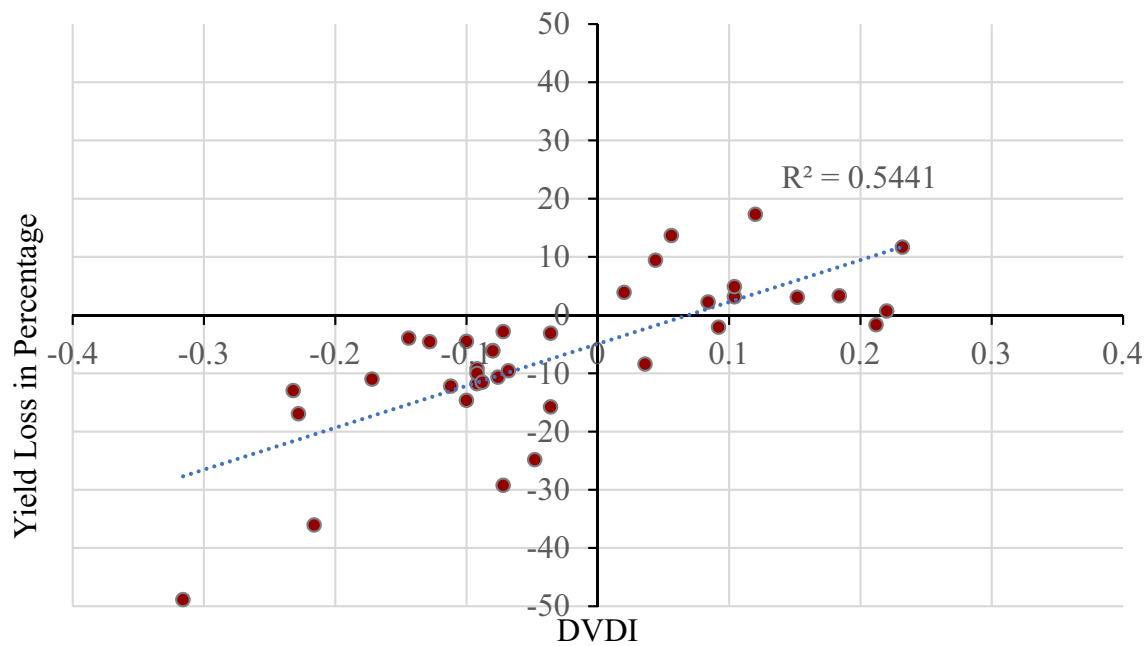


Fig. 14 Relationship between Disaster Vegetation Damage Index (DVDI) and crop yield loss

Table 1 Damage class and corresponding yield loss in percentage

	Yield loss in percentage						Total number of plots
	No loss	0–10%	10–20%	20–30%	30–40%	> 40%	
No damage	11	3	0	0	0	0	14
Very slight	0	8	5	2	0	0	15
Slight	0	2	2	0	0	0	4
Moderate	0	0	2	0	1	0	3
Severe	0	0	0	0	0	1	1
Very severe	0	0	0	0	0	0	0
Total Number of Plots	11	13	9	2	1	1	37

unavailable in most of the cases. Although our research considered two validation approaches, both have significant limitations. Pixel-level validation is biased to some extent, since estimated DVDI is inherited from NDVI change. However, validation of DVDI classes through NDVI changes is still meaningful, since it shows how DVDI subjective classes follow the drop in NDVI profile. We conducted plot-level validation by using available data from different seed companies, which data necessarily is the subject of cautious judgment because of the business motives of the companies and associated crop insurance issues. Seed companies may release yield data only for these plots that have the best yield records. Moreover, there is a high chance that these companies do not provide yield information for those plots that are severely affected by floods. Plot boundary information and accurate plot-level

loss information could significantly enhance the validation process. Despite having limitations and weaknesses, DVDI can be used successfully for the rapid assessment of flood crop damage.

Apart from these limitations, there are several advantages in the use of DVDI for crop damage assessment. First, the whole workflow mostly depends on free of charge available remote sensing data; thus, it can be applied anywhere at any time of the season. Second, this approach does not require survey data and historical data that are scarce in many developing countries. Third, this approach is able to provide a quick assessment immediately after flood events, which is precious for policy and decision making to reduce disaster risk. Although our study used historic crop rotation patterns for mapping crop types, if historic field-level crop information is unavailable, we

would suggest the use of in-season remote sensing-based crop mapping. Therefore our approach is useful for both developed and developing countries. Third, the approach used in our study is rapid and is useful for quick damage assessment to support immediate policy and decision making.

Acknowledgments This research was funded by grants from NASA Applied Science Program (Grant # NNX14AP91G, PI: Prof. Liping Di) and NSF INFEWS program (Grant # CNS-1739705, PI: Prof. Liping Di). Authors would like to thank seedling companies including Pioneer Hi-Bred International, Inc., Beck's, Syngenta, Bayer Global, and Golden Harvest Seeds for their portals for crop yield information. We are grateful to Hossain Mohiuddin, Zhi Chen, and Reuben Grandon of the University of Iowa for their assistance during field data collection in Iowa. We would like to express our special thanks to United States Department of Agriculture (USDA) for the Cropland Data Layer (CDL).

Open Access This article is licensed under a Creative Commons Attribution 4.0 International License, which permits use, sharing, adaptation, distribution and reproduction in any medium or format, as long as you give appropriate credit to the original author(s) and the source, provide a link to the Creative Commons licence, and indicate if changes were made. The images or other third party material in this article are included in the article's Creative Commons licence, unless indicated otherwise in a credit line to the material. If material is not included in the article's Creative Commons licence and your intended use is not permitted by statutory regulation or exceeds the permitted use, you will need to obtain permission directly from the copyright holder. To view a copy of this licence, visit <http://creativecommons.org/licenses/by/4.0/>.

References

- Adnan, M.S.G., A.Y.M. Abdullah, A. Dewan, and J.W. Hall. 2020. The effects of changing land use and flood hazard on poverty in coastal Bangladesh. *Land Use Policy* 99: Article 104868.
- Aerts, J.C.J.H., and W.J.W. Botzen. 2011. Climate change impacts on pricing long-term flood insurance: A comprehensive study for the Netherlands. *Global Environmental Change* 21(3): 1045–1060.
- Ahmed, M.R., K.R. Rahaman, A. Kok, and Q.K. Hassan. 2017. Remote sensing-based quantification of the impact of flash flooding on the rice production: A case study over northeastern Bangladesh. *Sensors* 17: Article 2347.
- Aurbacher, J., and S. Dabbert. 2011. Generating crop sequences in land-use models using maximum entropy and Markov chains. *Agricultural Systems* 104(6): 470–479.
- Bouwer, L.M. 2011. Have disaster losses increased due to anthropogenic climate change? *Bulletin of the American Meteorological Society* 92(1): 39–46.
- Brémond, P., and A. Agenais. 2013. Flood damage assessment on agricultural areas: Review and analysis of existing methods. <https://core.ac.uk/download/pdf/52629325.pdf>. Accessed 20 May 2019.
- Capellades, M.A., S. Reigber, and M. Kunze. 2009. Storm damage assessment support service in the U.S. corn belt using RapidEye satellite imagery. In *Remote sensing for agriculture, ecosystems, and hydrology XI*, Proceedings of a meeting held 1–3 September 2009, Berlin, Germany, SPIE Proceedings 7472, ed. C.M.U. Neale, and A. Maltese, 747208.1–747208.14. Bellingham, WA: SPIE (International Society for Optics and Photonics).
- Chejarla, V.R., V.R. Mandla, G. Palanisamy, and M. Choudhary. 2016. Estimation of damage to agriculture biomass due to Hudhud cyclone and carbon stock assessment in cyclone affected areas using Landsat-8. *Geocarto International* 32(6): 1–14.
- Chowdhury, E.H., and Q.K. Hassan. 2017. Use of remote sensing data in comprehending an extremely unusual flooding event over southwest Bangladesh. *Natural Hazards* 88(3): 1805–1823.
- Citeau, J.M. 2003. A new control concept in the Oise catchment area: Definition and assessment of flood compatible agricultural activities. In *Proceedings of FIG Working Week Conference*, 13–17 April 2003, Paris, France. Session TS 14 (14:00–15:30)—New Professional Tasks: Environmental Issues and Statutory Valuation. https://www.fig.net/resources/proceedings/fig_proceedings/fig_2003/TS_14/TS14_5_Citeau.pdf. Accessed 7 Sept 2020.
- Clement, M.A., C.G. Kilsby, and P. Moore. 2018. Multi-temporal synthetic aperture radar flood mapping using change detection. *Journal of Flood Risk Management* 11(2): 152–168.
- Cressman, D.R., M.H.P. Fortin, M.J. Hensel, P.H. Brubacher, and R.A. McBride. 1988. Estimation of cropland damages caused by overland flooding, two case studies. *Canadian Water Resources Journal* 13(3): 15–25.
- Del Ninno, C., P.A. Dorosh, and L.C. Smith. 2003. Public policy, markets and household coping strategies in Bangladesh: Avoiding a food security crisis following the 1998 floods. *World Development* 31(7): 1221–1238.
- Di, L., E.G. Yu, L. Kang, R. Shrestha, and Y. Bai. 2017. RF-CLASS: A remote-sensing-based flood crop loss assessment cyber-service system for supporting crop statistics and insurance decision-making. *Journal of Integrative Agriculture* 16(2): 408–423.
- Di, S., L. Guo, and L. Lin. 2018. Rapid estimation of flood crop loss by using DVDI. *2018 7th International Conference on Agro-geoinformatics (Agro-geoinformatics)*, 6–9 August 2018, Hangzhou, China. <https://doi.org/10.1109/agro-geoinformatics.2018.8476083>.
- Di, L., E. Yu, R. Shrestha, and L. Lin. 2018. DVDI: A new remotely sensed index for measuring vegetation damage caused by natural disasters. In *Proceedings of IGARSS 2018—The 2018 IEEE International Geoscience and Remote Sensing Symposium*, 22–27 July 2018, Valencia, Spain, 9067–9069. Piscataway, NJ: Institute of Electrical and Electronics Engineers (IEEE) <https://ieeexplore.ieee.org/document/8518022>. Accessed 11 Feb 2019.
- Dutta, D., S. Herath, and K. Musiaka. 2003. A mathematical model for flood loss estimation. *Journal of Hydrology* 277(1–2): 24–49.
- FAO (Food and Agriculture Organization). 2015. *The impact of disasters on agriculture and food security*. Rome: Food and Agriculture Organization of the United Nations.
- FEMA (Federal Emergency Management Agency). 2016. Texas severe storms and flooding (FEMA DR-4272). <https://www.fema.gov/sites/default/files/2020-09/PDAReportFEMA4272DRTX.pdf>. Accessed 10 Nov 2018.
- FEMA (Federal Emergency Management Agency). 2018a. Preliminary damage assessment report, Iowa severe storms, tornadoes, straight-line winds, and flooding (FEMA DR-4386). <https://www.fema.gov/sites/default/files/2020-03/FEMA4386DRIA.pdf>. Accessed 24 May 2019.
- FEMA (Federal Emergency Management Agency). 2018b. Preliminary damage assessment report, Nebraska severe storms, tornadoes, straight-line winds, and flooding (FEMA DR-4387). <https://www.fema.gov/sites/default/files/2020-03/FEMA4387DRNE.pdf>. Accessed 24 May 2019.
- Field, C.B., V. Barros, T.F. Stocker, and D. Qin. 2012. *Managing the risks of extreme events and disasters to advance climate change*

- adaptation: *Special report of the intergovernmental panel on climate change*. Cambridge: Cambridge University Press.
- Förster, S., B. Kuhlmann, K.E. Lindenschmidt, and A. Bronstert. 2008. Assessing flood risk for a rural detention area. *Natural Hazards and Earth System Science* 8: 311–322.
- Gerl, T., H. Kreibich, G. Franco, D. Marechal, and K. Schröter. 2016. A review of flood loss models as basis for harmonization and benchmarking. *PLoS One* 11(7): Article e0159791.
- Hirabayashi, Y., R. Mahendran, S. Koirala, L. Konoshima, D. Yamazaki, S. Watanabe, H. Kim, and S. Kanae. 2013. Global flood risk under climate change. *Nature Climate Change* 3(9): 816–821.
- Islam, M.M., and K. Sado. 2000. Flood hazard assessment in Bangladesh using NOAA AVHRR data with geographical information system. *Hydrological Processes* 14(3): 605–620.
- Kogan, F., L. Salazar, and L. Roytman. 2012. Forecasting crop production using satellite-based vegetation health indices in Kansas, USA. *International Journal of Remote Sensing* 33(9): 2798–2814.
- Lin, L., L. Di, E.G. Yu, L. Kang, R. Shrestha, M.S. Rahman, J. Tang, M. Deng, et al. 2016. A review of remote sensing in flood assessment. In *Proceedings of the 2016 Fifth International Conference on Agro-Geoinformatics*, 18–20 July 2016, Tianjin, China.
- Liu, W., J. Huang, C. Wei, X. Wang, L. R. Mansaray, J. Han, D. Zhang, and Y. Chen. 2018. Mapping water-logging damage on winter wheat at parcel level using high spatial resolution satellite data. *ISPRS Journal of Photogrammetry and Remote Sensing* 142: 243–256.
- Lu, L., C. Wu, and L. Di. 2020. Exploring the spatial characteristics of typhoon-induced vegetation damages in the southeast coastal area of China from 2000 to 2018. *Remote Sensing* 12(10). <https://doi.org/10.3390/rs12101692>.
- Merz, B., H. Kreibich, R. Schwarze, and A. Thielen. 2010. Assessment of economic flood damage. *Natural Hazards and Earth System Sciences* 10(8): 1697–1724.
- Mosleh, M.K., Q.K. Hassan, and E.H. Chowdhury. 2015. Application of remote sensors in mapping rice area and forecasting its production: A review. *Sensors* 15(1): 769–791.
- Okamoto, K., S. Yamakawa, and H. Kawashima. 1998. Estimation of flood damage to rice production in North Korea in 1995. *International Journal of Remote Sensing* 19(2): 365–371.
- Opolot, E. 2013. Application of remote sensing and geographical information systems in flood management: A review. *Research Journal of Applied Sciences Engineering and Technology* 6(10): 1884–1894.
- Osman, J., J. Inglada, and J.F. Dejoux. 2015. Assessment of a Markov logic model of crop rotations for early crop mapping. *Computers and Electronics in Agriculture* 113: 234–243.
- Ostu, N. 1979. A threshold selection method from gray-level histogram. *IEEE Transactions on Systems, Man, and Cybernetics* 9(1): 62–66.
- Rahman, M.S., and L. Di. 2017. The state of the art of spaceborne remote sensing in flood management. *Natural Hazards* 85(2): 1223–1248.
- Rahman, M.S., and L. Di. 2020. A systematic review on case studies of remote-sensing-based flood crop loss assessment. *Agriculture* 10(4): Article 131.
- Rahman, M.S., L. Di, R. Shrestha, E.G. Yu, L. Lin, L. Kang, and M. Deng. 2016. Comparison of selected noise reduction techniques for MODIS daily NDVI: An empirical analysis on corn and soybean. In *Proceedings of the 2016 Fifth International Conference on Agro-Geoinformatics*, 18–20 July 2016, Tianjin, China. Piscataway, NJ: Institute of Electrical and Electronics Engineers (IEEE).
- Rahman, M.S., L. Di, E.G. Yu, C. Zhang, and H. Mohiuddin. 2019. In-season major crop-type identification for US cropland from landsat images using crop-rotation pattern and progressive data classification. *Agriculture* 9(1): Article 17.
- Schumann, G.J.P., and D.K. Moller. 2015. Microwave remote sensing of flood inundation. *Physics and Chemistry of the Earth, Parts A/B/C* 83–84: 84–95.
- Shrestha, R., L. Di, E. G. Yu, L. Kang, L. Li, M. S. Rahman, M. Deng, and Z. Yang. 2016. Regression based corn yield assessment using MODIS based daily NDVI in Iowa state. In *Proceedings of the 2016 Fifth International Conference on Agro-Geoinformatics*, 18–20 July 2016, Tianjin, China. Piscataway, NJ: Institute of Electrical and Electronics Engineers (IEEE).
- Shrestha, R. 2017. A remote sensing-derived corn yield assessment model. Ph.D. thesis. George Mason University, Fairfax, Virginia, USA.
- Shrestha, R., L. Di, E.G. Yu, L. Kang, Y.Z. Shao, and Y. Bai. 2017. Regression model to estimate flood impact on corn yield using MODIS NDVI and USDA cropland data layer. *Journal of Integrative Agriculture* 16(2): 398–407.
- Shrestha, R., L. Di, E.G. Yu, Y. Shao, L. Kang, and B. Zhang. 2013. Detection of flood and its impact on crops using NDVI – Corn case. In *Proceedings of the 2013 Second International Conference on Agro-Geoinformatics*, 12–16 August 2013, Fairfax, VA, USA. Piscataway, NJ: Institute of Electrical and Electronics Engineers (IEEE).
- Tapia-Silva, F.M., S. Itzerott, S. Foerster, B. Kuhlmann, and H. Kreibich. 2011. Estimation of flood losses to agricultural crops using remote sensing. *Physics and Chemistry of the Earth, Parts A/B/C* 36(7–8): 253–265.
- USDA-ERS (United States Department of Agriculture–Economic Research Service). 2016. Crop production is concentrated in California and the Midwest. Washington, DC: United States Department of Agriculture – Economic Research Services. <https://www.ers.usda.gov/data-products/chart-gallery/gallery/chart-detail/?chartId=58320>. Accessed 6 Aug 2020.
- Xu, H. 2006. Modification of normalised difference water index (NDWI) to enhance open water features in remotely sensed imagery. *International Journal of Remote Sensing* 27(14): 3025–3033.
- Yu, E.G., L. Di, B. Zhang, Y. Shao, R. Shrestha, and L. Kang. 2013. Remote-sensing-based flood damage estimation using crop condition profiles. In *Proceedings of 2013 Second International Conference on Agro-Geoinformatics*, 12–16 August 2013, Fairfax, VA, USA. Piscataway, NJ: Institute of Electrical and Electronics Engineers (IEEE).
- Zhu, Q., X. Chen, H. Yang, and Z. Huang. 2007. A mathematical model for flood loss estimation based on spatial grid. In *Geoinformatics 2007: Geospatial Information Technology and Applications*. Proceedings of a meeting held 25–27 May 2007, Nanjing, China; Proceedings of SPIE Volume 6754, ed. P. Gong, 67541R-1–67541R-8. Bellingham, WA: SPIE (International Society for Optics and Photonics).